Polymer Chemistry

ROYAL SOCIETY OF CHEMISTRY

PAPER

View Article Online
View Journal | View Issue

Check for updates

Cite this: *Polym. Chem.*, 2025, **16**, 4250

One-pot route to aryl halide/sulfur/olefin terpolymers *via* sequential crosslinking by radical-initiated aryl halide-sulfur polymerization, inverse vulcanization, and sulfenyl chloride formation

Nawoda L. Kapuge Dona and Rhett C. Smith *

High sulfur content materials (HSMs) are gaining attention as sustainable and versatile polymers due to their high sulfur content, low-cost feedstocks, and promising applications in energy storage, catalysis, sorbents, and structural composites. This work presents a sequential crosslinking strategy that combines three known sulfur–carbon bond-forming mechanisms—radical-initiated aryl halide sulfur polymerization (RASP), inverse vulcanization (InV), and sulfenyl chloride formation—to prepare high-performance HSM terpolymers. Specifically, elemental sulfur was first reacted with 2,4-dichloro-3,5-dimethylphenol (**DDP**) *via* RASP, forming polymer $\mathbf{DS_{81}}$ and byproduct S_2Cl_2. Rather than discarding this toxic byproduct, *O*,*O*′-diallylbisphenol A (ABPA) was added to form sulfenyl chloride linkages in a single pot, yielding terpolymer $\mathbf{DAClS_{51}}$. Control polymers $\mathbf{DAS_{50}}$ (without S_2Cl_2) and $\mathbf{AS_{50}}$ (*via* traditional InV) were also synthesized. A comprehensive suite of physicochemical analyses confirmed that sequential crosslinking allows remarkable property tuning and efficient byproduct valorization. Thermogravimetric analysis (TGA) showed that $\mathbf{DAClS_{51}}$ and $\mathbf{DAS_{50}}$ exhibit higher char yields (≥40 wt% at 800 °C) than single-step materials, underscoring the stabilizing effect of their crosslinked aromatic components. Differential scanning calorimetry (DSC) confirmed $\mathbf{DAClS_{51}}$ had the highest glass transition temperature (36 °C), indicating increased crosslink density to the control polymers. SEM/EDX analysis confirmed uniform elemental distribution and residual chlorine in $\mathbf{DAClS_{51}}$, verifying successful utilization of *in situ* S_2Cl_2. $\mathbf{DAClS_{51}}$ also displayed the best mechanical properties, with flexural strength of 3.02 MPa and storage modulus of 357 MPa at 25 °C. This work showcases a potential route to synthesis HSMs by valorizing S_2Cl_2 and tuning properties *via* feedstock selection. It highlights the potential of integrated sulfur–carbon bond-forming strategies in sustainable polymer design and offers a pathway to address global sulfur surpluses through advanced material development.

Received 3rd June 2025,
Accepted 29th August 2025

DOI: 10.1039/d5py00548e

rsc.li/polymers

Open Access Article. Published on 04 September 2025. Downloaded on 2/1/2026 10:21:47 PM.
This article is licensed under a Creative Commons Attribution 3.0 Unported Licence.

Introduction

High sulfur content materials (HSMs) are emergent materials that contribute positively to sustainability goals through the utilization of elemental sulfur that is produced in megaton quantities as a byproduct of fossil fuel refining.[4–6] HSMs have found a panoply of applications ranging from battery manufacturing[7–17] and IR optics[18–23] to water purification adsorbents,[24–41] self-healing materials,[42–45] fertilizers,[46–48] pesticides,[49] and structural polymers.[50–66] The flurry of interest in HSMs is a result of Pyun's seminal contribution to the field in 2013, when the concept of inverse vulcanization was disclosed as a facile way to prepare HSMs from olefins and 50–99 wt% elemental sulfur.[13] In its simplest form, inverse vulcanization is the addition of sulfur atoms to olefin carbons (an example is provided in Scheme 1A).[2]

Inverse vulcanization has been employed to prepare HSMs from a wide range of petrochemical[35,67–76] and bio-derived olefins.[14,31,77–94] Advances in inverse vulcanization have been made to include catalytic,[95,96] mechanochemical,[97–99] photochemical,[100,101] and organic solution-phase[102] methodologies. Other strategies have been discovered that lower reaction temperatures,[2] improve processibility,[43,103,104] or increase mechanical strength[105] of resultant HSMs. Insights into mechanistic aspects of inverse vulcanization[106] and the complex composition of HSMs[107,108] have further contributed to our understanding of this fascinating class of materials.

Burgeoning interest in applications of HSMs has been accompanied by significant efforts to expand the scope of organic substrates for their preparation beyond olefins.

Department of Chemistry, Clemson University, Clemson, South Carolina, 29634, USA. E-mail: rhett@clemson.edu

This journal is © The Royal Society of Chemistry 2025

Open Access Article. Published on 04 September 2025. Downloaded on 2/1/2026 10:21:47 PM.
This article is licensed under a Creative Commons Attribution 3.0 Unported Licence.

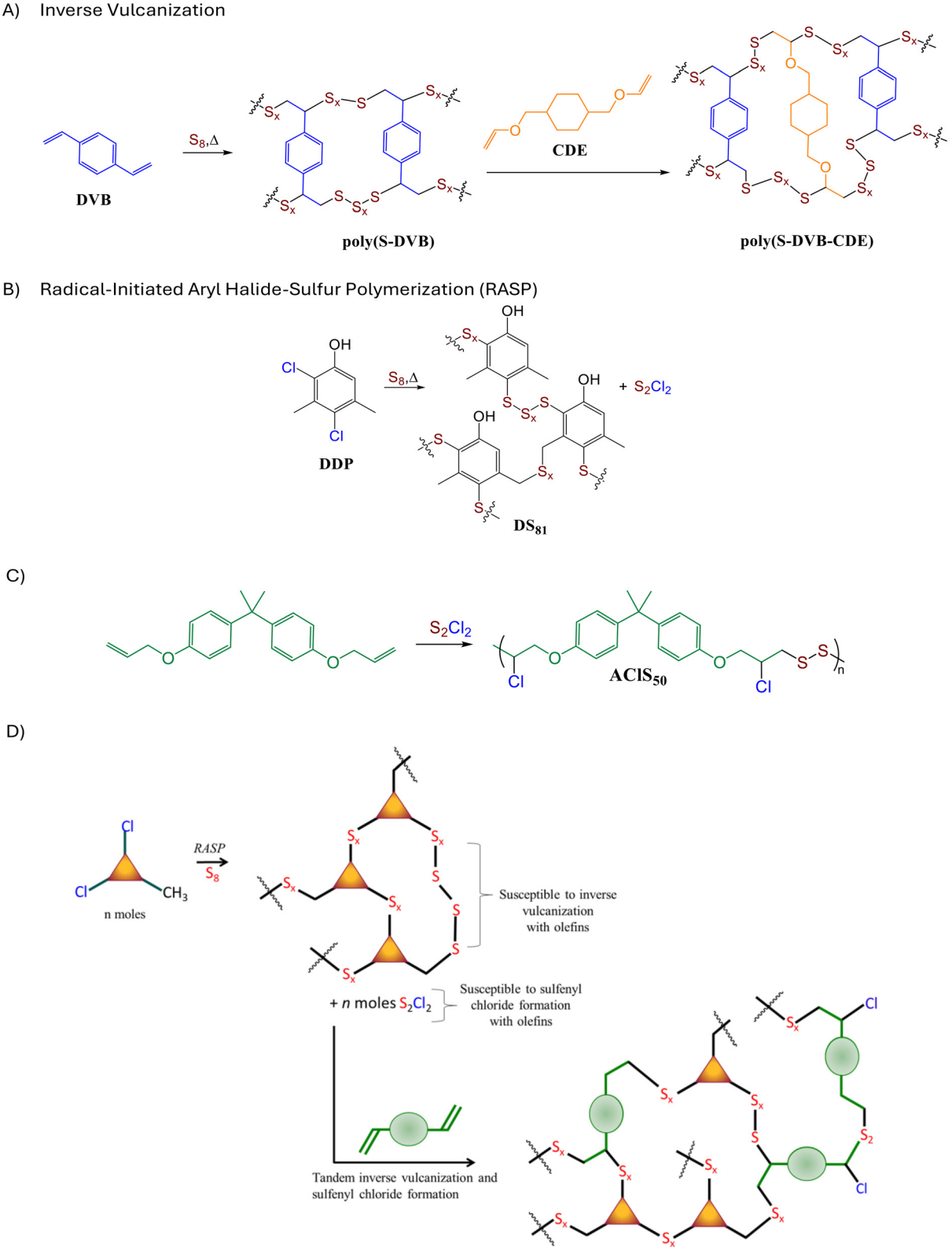

Scheme 1 (A) High sulfur-content material **poly(s-DVB)** is formed by olefin addition of elemental sulfur to olefins (inverse vulcanization). This material undergoes an additional inverse vulcanization reaction when a second olefin, **CDE**, is added. Whereas temperatures of ~180 °C are generally required for the first crosslinking step, the second cross-linking step can occur at as low as 90 °C.[2] (B) Previously-reported preparation of $\mathbf{DS_{81}}$ by the RASP process.[3] (C) Previously-reported use of S_2Cl_2 to form sulfenyl chloride linkages to prepare $ACIS_{50}$ (A indicating the ABPA monomer, Cl and S indicating the atoms added to the olefin, and 50 indicating that 50% of the repeat units are ABPA).[1] (D) Schematic representation of the sequential crosslinking process described herein.

Open Access Article. Published on 04 September 2025. Downloaded on 2/1/2026 10:21:47 PM.
This article is licensed under a Creative Commons Attribution 3.0 Unported Licence.

Elemental sulfur reacts with 1,3,5-triisopropylbenzene, for example, to form polymers *via* S–$C_{benzylic}$ bond formation.[109] S–C_{aryl} bond-forming reactions between elemental sulfur and anisole derivatives have been discovered that facilitate preparing HSMs from waste plastic and lignin derivatives.[110–118]

Most relevant to the current study, Karunarathna, *et al.* reported a modification of the MacCallum polymerization wherein aryl halides are polymerized with sulfur, a process referred to as radical-initiated aryl halide sulfur polymerization (RASP, an example of which is provided in Scheme 1B).[3,111,114] In RASP, the HSM product is accompanied by 0.5 mol equivalent of S_2Cl_2 per mole of halide, as illustrated in Scheme 2 for polymerization of 2,4-dichloro-3,5-dimethylphenol (**DDP**) *via* RASP. Production of toxic and corrosive S_2Cl_2 lowers the atom economy, increases separation and disposal costs, and detracts from the greenness of RASP.

Pyun recently reported that S_2Cl_2 can be used as a reactant with olefins to produce polymers *via* S–C bond formation (an

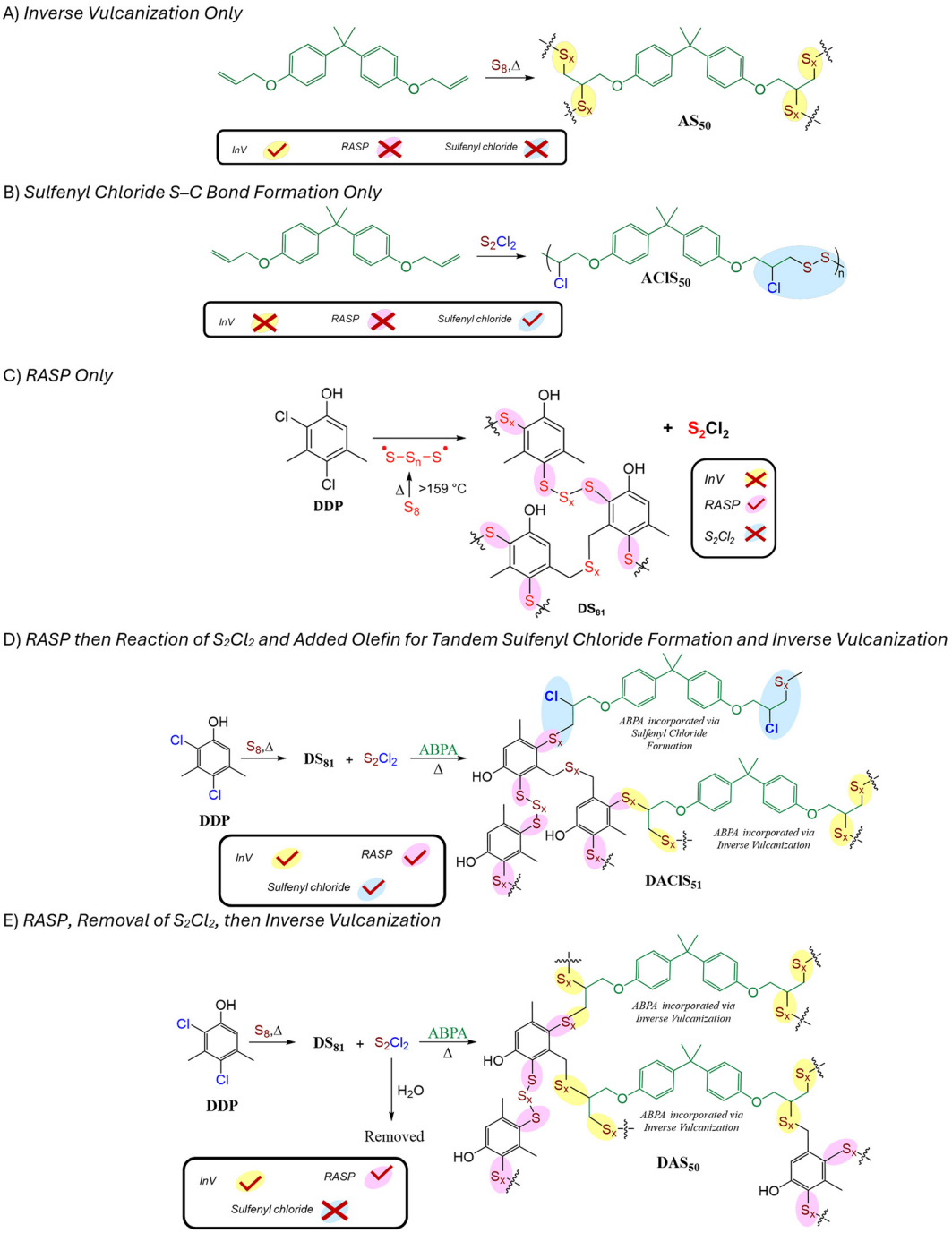

Scheme 2 The current work involves the preparation of (A) $\mathbf{AS_{50}}$, (B) $\mathbf{DAS_{50}}$ and (C) $\mathbf{DACIS_{51}}$ to illustrate the extent to which application of different combinations of known S–C bond-forming mechanisms and composition can be leveraged to tune polymer properties.

 This journal is © The Royal Society of Chemistry 2025

Open Access Article. Published on 04 September 2025. Downloaded on 2/1/2026 10:21:47 PM. This article is licensed under a Creative Commons Attribution 3.0 Unported Licence.

example is shown in Scheme 1C). Detailed NMR spectroscopic analysis of model reactions indicated the formation of both Markovnikov and anti-Markovnikov regioisomers, with a notable preference for anti-Markovnikov addition.[1]

This reactivity of S_2Cl_2 with olefins led us to envision the sequential crosslinking process schematically depicted in Scheme 1D involving (1) RASP to form S–C_{aryl} bonds; then (2) addition of an olefin to the crude S_2Cl_2-containing mixture, leading to sulfenyl chloride formation. Step 2 of the sequential crosslinking would be accompanied by inverse vulcanization reactions analogous to those occurring after addition of **CDE** depicted in Scheme 1A.

The hypothesized sequential crosslinking simultaneously has the potential for property tuning by varying the identity and amount of the added olefin and consumes the S_2Cl_2 side product of the initial RASP step.

Herein, the sequential crosslinking strategy was employed to prepare terpolymers by reactions of elemental sulfur with 2,4-dichloro-3,5-dimethylphenol (**DDP**) as the aryl halide comonomer and *O*,*O*′-diallylbisphenol A (ABPA) as the olefin comonomer (Scheme 2). Both **DDP** and ABPA were selected for their well-established reactivity, structural diversity, and their ability to form polymers with diverse thermal and mechanical properties. Additionally, **DDP** serves as a chloro-lignin model compound that can be rapidly synthesized from abundant xylyl alcohol through a green reaction and affordable. ABPA is a derivative of BPA, a widely used monomer in the production of petroleum-derived plastics. To assess the extent to which S_2Cl_2 contributes to terpolymer properties, a control experiment was undertaken in which S_2Cl_2 was hydrolyzed and extracted prior to the addition of the olefin (Scheme 2C). The chemical, thermal, morphological, and mechanical properties of terpolymers were evaluated for comparison to those of $\mathbf{DS_{81}}$. As anticipated, each terpolymer resulting from the post-polymerization modification of $\mathbf{DS_{81}}$ exhibited distinctly different properties. This proof-of-process study thus demonstrated a simple method for harnessing and thus eliminating a toxic side product of RASP in a productive manner while simultaneously providing an avenue for tuning the properties of the resultant HSMs.

Results and discussion

Design, synthesis, and chemical characterization

The overarching goal of this study was to assess the extent to which sequential crosslinking involving RASP, sulfenyl chloride formation, and inverse vulcanization could be used to tune the properties of the resulting polymers, and the extent to which each of these processes contributes to those properties. For the current study, the first step was RASP of 2,4-dichloro-3,5-dimethylphenol (**DDP**) with elemental sulfur as previously reported[3] to give poly(S-*ran*-DPP), herein abbreviated $\mathbf{DS_{81}}$ (Scheme 2C; D indicates DPP comonomer, S indicates sulfur comonomer, and 81 denotes the wt% of S in this polymer). This reaction generates one equivalent of S_2Cl_2 for each equivalent of **DDP**. The reaction mixture was cooled to room temperature under dry nitrogen prior to adding *O*,*O*′-diallylbisphenol A (ABPA) *via* syringe to the crude reaction mixture resulting from step 1 (Scheme 2D) and then heating was resumed. This yielded poly[S-*ran*-**DDP**-*ran*-(C_3H_5Cl-BPA-C_3H_5Cl)] (abbreviated $\mathbf{DAClS_{51}}$, where D indicates **DDP** comonomers, A indicates ABPA comonomers, Cl indicates the presence of Cl in the polymer backbone, S indicates sulfur comonomer, and 51 denotes the wt% of sulfur in the polymer). As a control, $\mathbf{DS_{81}}$ was isolated (by hydrolysis and extraction of the S_2Cl_2 side product) followed by heating of isolated $\mathbf{DS_{81}}$ with ABPA to give poly[S-*ran*-**DDP**-*ran*-(C_3H_5-BPA-C_3H_5)] (abbreviated $\mathbf{DAS_{50}}$, where D indicates **DDP** comonomers, A indicates ABPA comonomers, S indicates sulfur comonomers, and 50 denotes the wt% of sulfur in the polymer). Formation of $\mathbf{DAS_{50}}$ (Scheme 2E) can be viewed as a control experiment because crosslinking by inverse vulcanization is still possible, but the absence of S_2Cl_2 precludes the contribution of sulfenyl chlorides. Finally, the reaction of ABPA with elemental sulfur to give poly[S-*ran*-(C_3H_5-BPA-C_3H_5)] (abbreviated $\mathbf{AS_{50}}$, where A indicates ABPA comonomers, S indicates sulfur comonomers, and 50 indicates the wt% of sulfur in the polymer) was undertaken to assess the properties of the copolymer of ABPA and elemental sulfur resulting exclusively from inverse vulcanization between these two comonomers (Scheme 2A). The copolymer of ABPA and S_2Cl_2 (Scheme 1C) was previously reported.[1] The $\mathbf{DAClS_{51}}$ and $\mathbf{DAS_{50}}$ polymers exhibited a glassy black and grey appearance, respectively, whereas the $\mathbf{AS_{50}}$ polymer appeared as a matte brown solid (Fig. 1). Notably, all composites demonstrated remeltability, allowing for the reshaping and fabrication of specimens suitable for mechanical property analysis. The four materials discussed herein can be categorized on the basis of the S–C bond-forming reactions involved in their formations as well as in terms of the comonomers incorporated into their backbones (Table 1).

Sulfur atoms in HSMs are generally incorporated as (1) oligo/polysulfide chains connected to organic components through C–S bonds or (2) oligo/polysulfide chains and rings entrapped within

Fig. 1 Terpolymers $\mathbf{DAClS_{51}}$ (A) exhibited a glassy black appearance, and $\mathbf{DAS_{50}}$ (B) had a glassy grey appearance, while $\mathbf{AS_{50}}$ (C) was a matte brown matte solid.

Table 1 Classification of materials discussed herein on the basis of the S–C bond-forming reactions used in their synthesis

	InV	RASP	Sulfenyl chloride formation
$\mathbf{AS_{50}}$	Yes	No	No
$\mathbf{DS_{81}}$	No	Yes	No
$\mathbf{DAS_{50}}$	Yes	Yes	No
$\mathbf{DAClS_{51}}$	Yes	Yes	Yes

Open Access Article. Published on 04 September 2025. Downloaded on 2/1/2026 10:21:47 PM. This article is licensed under a Creative Commons Attribution 3.0 Unported Licence.

the crosslinked network but not covalently linked to organic comonomers. The mixture of entrapped sulfur species is known as "dark sulfur".[107,108] Although dark sulfur is challenging to differentiate from bonded sulfides using techniques like IR and ^{1}H NMR spectroscopy, Hasell's group reported a convenient method for its quantification using UV-visible spectroscopy. In this method extractable sulfur is quantified by UV-vis absorption. This analysis revealed dark sulfur content percentages of 3.3 wt% for **DAClS$_{51}$** and 18.5 wt% for **DAS$_{50}$**, and 57% for **DS$_{81}$** (Table 2). These data confirm progressively greater involvement of sulfur atoms in organic-bound crosslinks (even accounting for the difference in total wt% S in the polymers), and consequently less dark sulfur, as progressively more S–C bond-forming mechanisms are employed. Lower amounts of physically entrapped dark sulfur also correlates with higher glass transition temperatures (T_g) determined from DSC data (Table 2).[108] **DS$_{81}$**, in which only S–C$_{aryl}$ and S–C$_{benzyl}$ crosslinks are made, has a T_g of −34 °C, typical of HSMs containing polymeric sulfur crosslinks. **DAS$_{50}$** additionally features S–C$_{alkyl}$ crosslinks formed by the addition of S radicals to ABPA olefins and has a T_g of 13 °C. **DAClS$_{51}$** features all of the crosslinking mechanisms observed in **DAS$_{50}$**, but also features S_2Cl_2-mediated crosslinking to afford –C(Cl)–C(H)–S–SC(H)–C(Cl)– crosslinks (and regioisomers resulting from a mixture of Markovnikov and anti-Markovnikov addition to the olefins) and has a considerably higher T_g of +36 °C.

The Fourier-transform infrared (FTIR) spectra of composites (Fig. S1 in SI) provided additional evidence for the proposed reactivity. Some peaks characteristics for the presence of **DDP** and ABPA comonomers were retained in spectra of both polymers, **DAClS$_{51}$** and **DAS$_{50}$**, including peaks at 844 cm^{-1} (out of plane aromatic C–H deformation), ~1373 cm^{-1} (C–H stretching), ~1165 cm^{-1} (C–O stretching) and ~1573 cm^{-1} (aromatic C=C stretching). Peaks at 584 and 705 cm^{-1} in the **DDP** spectrum, attributable to C–Cl stretches, are reduced in the spectra for its composite polymers compared to **DDP**, indicating the replacement of chloride substituents through the RASP mechanism. Peaks at 3032 cm^{-1} (allyl C=C–H stretching), 1647 cm^{-1} (C=C stretching), and 921 cm^{-1} (C=C–H bending) that are responsible for olefinic functionalities in the ABPA spectrum are diminished in the spectra for its composite polymers, indicating the successful reaction of ABPA olefins with sulfur and *in situ*-generated S_2Cl_2.

Scanning electron microscopy (SEM) imaging with energy-dispersive X-ray analysis (EDX) was employed to investigate the microstructure and elemental composition of the synthesized materials (Fig. 2 and Fig. S2–5 in the SI). This study confirmed the homogeneous nature of bulk **DAClS$_{51}$** and **DAS$_{50}$**, revealing uniform distributions of elemental components. Specifically, **DAClS$_{51}$** exhibited consistent distributions of carbon, oxygen, sulfur, and chlorine, indicating the successful incorporation of S_2Cl_2 through olefinic units in ABPA. Conversely, **DAS$_{50}$** displayed uniform distributions of carbon, oxygen, and sulfur, but no detectable Cl, suggesting the effective removal of S_2Cl_2 from the polymer matrix.

Elemental composition from combustion analysis generally agreed well with expected values (see Experimental section for details). For **DAClS$_{51}$**, it was especially important to confirm the proposed incorporation of Cl due to reaction of *in situ*-generated S_2Cl_2. Elemental contributions by C, H, and S (C, 38.46; S, 50.93; H, 2.49%) agreed well with the theoretical (C, 36.30; S, 47.72; Cl, 7.59; H, 3.36%.). Elemental compositions found

Table 2 Thermal and morphological properties of the **DAClS$_{51}$** and **DAS$_{50}$** compared to **DS$_{81}$** and S$_8$

Materials	T_d [a] / °C	T_m [b] / °C	$T_{g,DSC}$ [c] / °C	Percent crystallinity[d]	Dark sulfur (wt%)
DAClS$_{51}$	223	116	36	66	3.0[e]
DAS$_{50}$	214	116	13	69	18[e]
AS$_{50}$	232	117	1.1	ND[f]	48[g]
DS$_{81}$	232	116	−34	18	57[g]
S$_8$	229	118	NA	100	NA

[a] The temperature at which 5% mass loss was observed by TGA. [b] The temperature at the peak maximum of the endothermic melting. [c] Glass transition temperature. [d] The reduction of the percent crystallinity of each sample was calculated with respect to sulfur (normalized to 100%). [e] Percent ethyl acetate-extractable sulfur species. [f] No cold crystallization peaks were observed by DSC. [g] Percent CS_2-extractable sulfur species.

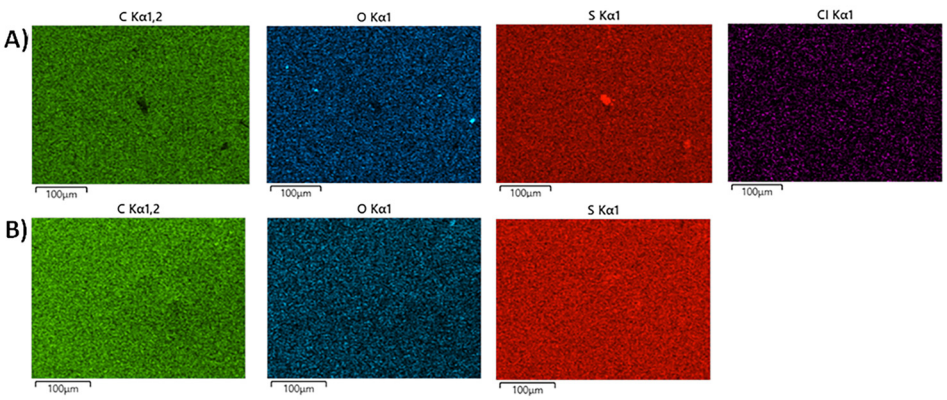

Fig. 2 Scanning electron microscopy with elemental mapping by energy dispersive X-ray analysis (SEM/EDX) of (A) **DAClS$_{51}$** and (B) **DAS$_{50}$**. Carbon is shown in green, oxygen in blue, sulfur in red, and chlorine in purple.

 This journal is © The Royal Society of Chemistry 2025

Open Access Article. Published on 04 September 2025. Downloaded on 2/1/2026 10:21:47 PM. This article is licensed under a Creative Commons Attribution 3.0 Unported Licence.

from EDS analysis (Fig. S3a) also agreed well (±1.5%) with the theoretical values for carbon and sulfur (C, 37.0; S, 50.5), though this analysis revealed chlorine content (5.0 ± 1.5%), indicating that 65–99% of the theoretical amount of chlorine (7.6%). This discrepancy suggests that while a significant portion of S_2Cl_2 was incorporated, some chlorine may have been lost due to the volatile nature of S_2Cl_2 or due to incomplete conversion during the reaction.

Thermal and morphological properties

Thermogravimetric analysis (TGA, Table 2, and Fig. S6 in SI) was used to determine the decomposition temperature of the products (T_d, here defined as the temperature at which 5% mass loss was observed). Determination of the T_d in HSMs wherein both entrapped orthorhombic sulfur and crosslinked sulfur provides insight into the thermal stability of the materials and the contributions of the different components in the material. In **DAClS$_{51}$** and **DAS$_{50}$**, the major decompositions were observed at 223 and 214 °C, respectively, due to the sublimation of elemental sulfur from the materials. Two decompositions were observed for **DS$_{81}$**, the first decomposition event at 232 °C due to the sublimation of sulfur and a second decomposition event at 470 °C due to the decomposition of the aryl-sulfide part of the polymer network. After incorporating ABPA, the **DAClS$_{51}$** and **DAS$_{50}$** composites showed higher char yield at 800 °C than most other HSMs due to the high aromatic content of the materials.

Differential scanning calorimetry (DSC, Table 2, and Fig. S7–10 in SI) was used to analyze **DAClS$_{51}$** and **DAS$_{50}$**, that revealed an endothermic melting peak at 116 °C attributable to the melting of orthorhombic sulfur in sulfur-rich domains of the composites. In **DAS$_{50}$**, a small shoulder in melting peak at 111 °C corresponded to phase change from the orthorhombic to the monoclinic allotrope of S_8. The heating curves for **DAClS$_{51}$** and **DAS$_{50}$** exhibited a broad glass transition (T_g) centered at 36 °C and 13 °C, respectively. In contrast, **AS$_{50}$** exhibited a T_g at 1.1 °C, consistent with shorter oligosulfur crosslinks in this material due to the presence of potentially four crosslinkable carbon sites in ABPA compared to fewer in the **DDP** monomer comprising a portion of the organic comonomers in **DS$_{81}$**. **DS$_{51}$**, composed of 51 wt% S_8 and 49 wt% **DDP**, exhibited T_g close to those of **DS$_{81}$** (−35 °C and −34 °C, respectively), which are lower than those of **DAClS$_{51}$**, **DAS$_{50}$**, and **AS$_{50}$**. This difference may be attributed to the formation of more crosslinks in ABPA-containing products, which restrict the movement of polymeric sulfur chains in the polymer network, leading to an increase in the T_g. Additionally, the incorporation of chlorine into high-density polyethylene (HDPE) has been shown to increase T_g due to restricted chain mobility and enhanced intermolecular interactions, suggesting a similar effect may contributeto the higher T_g observed in **DAClS$_{51}$**.[119] Small cold crystallization peaks at 64 and 86 °C are also observed for **DAClS$_{51}$** and **DAS$_{50}$** attributable to the partial organization of polymer chains and reflect the partial organization of polysulfur chains. **AS$_{50}$** does not show cold crystallization peaks in its DSC thermogram, consistent with the lack of polymeric sulfur crosslinking chains. The melting and cold crystallization enthalpies determined from the DSC traces were used to calculate the percent crystallinity of materials relative to crystalline orthorhombic sulfur. The percent crystallinity of the **DAClS$_{51}$** and **DAS$_{50}$** were 66% and 69%, which are comparatively higher than previous HSMs, including **DS$_{81}$** (18% crystallinity), while **AS$_{50}$** does not show cold crystallization features in the DSC thermogram.

Table 3 Mechanical properties of the **DAClS$_{51}$** and **DAS$_{50}$** compared to other HSMs

Materials	E' at 25 °C (MPa)	Flexural strength/modulus (MPa)
DAClS$_{51}$	357	3.02 ± 0.3/62 ± 10
DAS$_{50}$	8.92	2.32 ± 0.5/207 ± 2.6
DS$_{81}$	338	2.0/240
AS$_{50}$ [a]	2.73	1.7 ± 0.3/22 ± 2[c]
LOS$_{90}$ [b]	439	5.7/186
S_8	ND[c]	ND[c]

[a] Composite made by reaction of *O*,*O*′-diallyl bisphenol A (50 wt%) and sulfur (50 wt%) heated at 250 °C. [b] Composite made by reaction of lignin oil (10 wt%) and elemental sulfur (90 wt%) heated at 230 °C. [c] Not determined.

Mechanical properties

The dynamic mechanical analysis (DMA) and flexural strength analysis provide crucial insights into the influence of composition and S–C bond forming mechanisms on mechanical behavior of **DAClS$_{51}$** and **DAS$_{50}$** copolymers. Rectangular sample specimens (Fig. S11 in SI) were used as test samples for DMA data (Fig. S13, 14 in SI, Table 3) over the temperature range of −60 to +80 °C to evaluate the temperature dependence of storage modulus (E'), loss modulus (E'') and damping factor ($\tan\delta$). At room temperature, **DAClS$_{51}$** and **DAS$_{50}$**, **DS$_{81}$**, and **AS$_{50}$** (composite prepared using 50 wt% ABPA and 50 wt% sulfur) exhibited 357 MPa, 8.92 MPa, 338 MPa and 2.73 MPa storage moduli, indicating the **DAS$_{50}$** and **AS$_{50}$** required less force for deformation. The polar covalent C–Cl bonds in **DAClS$_{51}$** enhance intermolecular interactions in **DAClS$_{51}$** *versus* **DAS$_{50}$**, which contribute to the higher modulus of **DAClS$_{51}$** compared to **DAS$_{50}$**. As a point of comparison, previously-reported **LOS$_{90}$**, a highly crosslinked composite prepared from 10 wt% lignin oil and 90 wt% elemental sulfur exhibited a storage modulus of 439 MPa, relatively close to that of **DAClS$_{51}$**, demonstrating the higher stiffness of the materials that may be an additive effect of crosslinking and incorporation of polar C–Cl bonds.[116] This observation aligns with prior studies on chlorinated polyethylene (CPE), where the introduction of C–Cl bonds into high density polyethylene (HDPE) was shown to increase the storage modulus due to microstructural interactions and formation of ordered domains within the polymer matrix.[119] These findings support the idea that polar covalent C–Cl bonds in **DAClS$_{51}$** can enhance intermolecular interactions and restrict segmental mobility, thereby increasing stiffness.

Flexural strength analysis of **DAClS$_{51}$** and **DAS$_{50}$** at room temperature revealed additional differences in the material properties (Table 3, stress–strain plots provided in Fig. S15 and 16 in SI), indicating that the flexural strengths for **DAClS$_{51}$** and

Open Access Article. Published on 04 September 2025. Downloaded on 2/1/2026 10:21:47 PM. This article is licensed under a Creative Commons Attribution 3.0 Unported Licence.

DAS_{50} are 3.02 MPa and 2.32 MPa, respectively. These data suggest an additional strengthening effect of crosslinking facilitated by S_2Cl_2 in **$DAClS_{51}$** *versus* **DAS_{50}**. The values for both sequentially crosslinked materials also exceeded the flexural strengths for **DS_{81}** (2.0 MPa) and **AS_{50}** (1.7 MPa) made by single crosslinking steps of the composite monomers.

Conclusions

This study presents the first investigation exploring a sequential crosslinking strategy to produce high sulfur-content terpolymers leveraging radical-initiated aryl halide sulfur polymerization (RASP), inverse vulcanization, and sulfenyl chloride S–C bond forming reactions. By reacting elemental sulfur with 2,4-dichloro-3,5-dimethylphenol (**DDP**) and *O*,*O*′-diallylbisphenol A (ABPA) organic comonomers, we successfully synthesized terpolymers having different thermal and mechanical properties, demonstrating the feasibility and advantages of this novel approach.

Mechanically, the dynamic mechanical analysis (DMA) and flexural strength tests highlighted the modest change in properties of the terpolymers, with **$DAClS_{51}$** showing slightly improved flexural strength and higher storage modulus compared to control samples. This enhanced flexural strength is comparable to that of construction materials made with ordinary Portland cement (3.7 MPa), highlighting the potential of these high sulfur content composites for future use in structural applications. These results suggest promising commercial potential, particularly in the construction industry, where sustainable alternatives to conventional materials are increasingly in demand. Additionally, the sequential crosslinking not only improved the material's mechanical performance but also effectively utilized the toxic S_2Cl_2 byproduct, demonstrating a dual benefit of property enhancement and environmental impact reduction.

The findings underscore the potential of the sequential crosslinking strategy to tailor polymer properties, offering a versatile and sustainable pathway for the development of high-performance HSMs. This approach not only addresses the challenges associated with sulfur byproducts but also provides a framework for future research to explore the vast combinatorial possibilities of sulfur and organic comonomers. Several additional studies are underway to assess the extent to which different olefin and aryl halide comonomers can be combined with elemental sulfur in similar sequential crosslinking processes to further tune the properties of resultant terpolymers. Furthermore, the impact of residual chlorine on recyclability, environmental stability, and end-of-life behaviour of these materials will be evaluated in future work.

Experimental section

Chemicals and materials

The 2,4-dichloro-3,5-dimethylphenol (>98.0%) and sulfur powder were purchased from TCI America and Dugas Diesel, USA, respectively. These chemicals were used without further purification. *O*,*O*′-Diallylbisphenol A (ABPA) was prepared following the previously reported method.[120] **DS_{81}** was prepared as previously reported and had elemental analysis found to be C, 16.5; S, 80.5; H, 0.3; Cl, 0.5%.[3]

General considerations

Thermogravimetric analysis (TGA, Mettler Toledo, Columbus, OH, USA) data were recorded on a TA SDT Q600 instrument over the range 25 to 800 °C, with a heating rate of 10 °C min^{-1} under a flow of N_2 (20 mL min^{-1}).

Differential scanning calorimetry (DSC) data were acquired (Mettler Toledo DSC 3 STARe System, Mettler Toledo, Columbus, OH, USA) over the range −60 to 140 °C with a heating rate of 10 °C min^{-1} under a flow of N_2 (200 mL min^{-1}). Each DSC measurement was carried out over three heat–cool cycles.

Dynamic Mechanical Analysis (DMA) and flexural strength analysis were performed using Mettler Toledo DMA 1 STARe System (Mettler Toledo, Columbus, OH, USA) in single cantilever mode. The powder of materials was cast from silicone resin molds (Smooth-On Oomoo® 30 platinum-cure) and heated in an oven for 1 h to prepare rectangular prisms. The samples were cured for 4 d, and the dimensions were approximately 1.5 × 10 × 18 mm. Sample dimensions were measured using a digital caliper with 0.01 mm resolution. The temperature range of −60 to 80 °C was used to obtain the temperature-dependent data with a heating rate of 5 °C min^{-1}. The samples were clamped with 1 cN m^{-1} force, and the results were collected with the measurement mode of displacement control with a displacement amplitude of 5 μm and a frequency of 1 Hz. The stress–strain analysis was performed isothermally at 25 °C. The clamping force was 1 cN m, and the performing force was varied from 0 to 10 N with a ramp rate of 0.2 N min^{-1}. Flexural analysis was performed in triplicate, and the results were averaged.

UV-vis data were collected using Simple Reads software on an Agilent Technologies Cary 60 UV-vis (Agilent Technologies, Inc. Santa Clara, CA, USA).

Fourier transform infrared spectra were obtained using a Shimadzu IR Affinity-1S instrument (Shimadzu Corporation, Columbia, MD, USA) with an ATR attachment operating over 400–4000 cm^{-1} at ambient temperature.

SEM and EDX were acquired on a Schottky Field Emission Scanning Electron Microscope SU5000 (Hitachi High-Tech, Tokyo, Japan) operating in variable pressure mode with an accelerating voltage of 15 keV.

Cautionary note on reaction of elemental sulfur with organics

Heating elemental sulfur with organics can result in the formation of H_2S or other gases. Such gases can be toxic, foul-smelling, and corrosive. Temperature must be carefully controlled to prevent thermal spikes that contribute to the potential for H_2S or other gas evolution. Rapid stirring, shortened heating times, and very slow addition of reagents can help avoid unforeseen temperature spikes. Heating elemental sulfur with aryl halides can produce various compounds of sulfur

 This journal is © The Royal Society of Chemistry 2025

Open Access Article. Published on 04 September 2025. Downloaded on 2/1/2026 10:21:47 PM. This article is licensed under a Creative Commons Attribution 3.0 Unported Licence.

and halogens. These species can be gases, highly volatile, toxic and/or corrosive.

Synthesis of AS_{50}

Elemental sulfur (5.00 g) was weighed directly into a 20 mL scintillation vial. The vessel was placed in a thermostat-equipped oil bath set to 250 °C. Once the sulfur turned a viscous dark red-orange color (indicative of thermal ring-opening), 5.01 g of ABPA was added. The reaction media was vigorously stirred with a Teflon-coated stir bar until the reaction mixture became homogenous. Once the reaction mixture was homogenous, the reaction solution was transferred to stainless steel molds in a 180 °C oven to cure for 16 h. Reagent masses and results of elemental combustion microanalysis are provided below. Recovered yield: 93%. Elemental analysis calculated: C, 40.89; S, 50.00; H, 3.92%. Found: C, 40.65; S, 50.75; H, 3.65%.

Synthesis of $DAClS_{51}$

Elemental sulfur (21.0 g) and 2,4-dichloro-3,5-dimethylphenol (9.00 g) were weighed directly into a Schlenk flask equipped with a Teflon-coated magnetic stir bar and a reflux condenser. The flask was then placed in an oil bath, heated to a temperature of 230 °C, and heated for 24 h with continuous stirring and purging nitrogen. After 24 h, the flask was cooled to ~130 °C. After cooling, *O*,*O*′-diallylbisphenol A (14.5 g, one mole equivalent with respect to **DDP**) was added slowly to the flask through the Schlenk line using a syringe. The oil bath temperature was increased to 180 °C and heated for 1.5 h with continuous stirring under a dynamic flow of nitrogen. After 1.5 h, the reaction mixture was cooled to room temperature and kept for another 16 h under dry nitrogen. The title compound was recovered as a black, glassy solid in quantitative yield. Elemental analysis calculated: C, 36.30; S, 47.72; Cl, 7.59; H, 3.36%. Found (combustion analysis): C, 38.46; S, 50.93; Cl, 5.0; H, 2.49% (Atlantic Microlab, Inc.); found (EDS): C, 37.0; S, 50.5; Cl, 5.0.

Synthesis of DAS_{50}

Elemental sulfur (14.0 g) and 2,4-dichloro-3,5-dimethylphenol (6.00 g) were weighed directly into a Schlenk flask equipped with a Teflon-coated magnetic stir bar and a reflux condenser. The flask was then placed in an oil bath, heated to a temperature of 230 °C, and heated for 24 h with continuous stirring and purging nitrogen. After 24 h, the flask was cooled, and the product was collected and crushed into a powder. Then, 30.0 mL of deionized water was added to the powdered product and continuously stirred at room temperature for 2 h to affect hydrolysis of the S_2Cl_2. After 2 h, the solid product was collected by filtration and rinsed with copious amounts of deionized water. The powder was then oven-dried at 60 °C overnight. After that, the dried product was again added into a Schlenk flask equipped with a Teflon-coated magnetic stir bar and a reflux condenser. The flask was then placed in an oil bath, heated to a temperature of 130 °C, and heated until DS_{81} melted with continuous stirring and purging under a flow of dry nitrogen gas. Then, *O*,*O*′-diallylbisphenol A (9.69 g, one mole equivalent with respect to **DDP**) was added slowly to the flask through the Schlenk line using a syringe. The oil bath temperature was increased to 180 °C and heated for 1.5 h with continuous stirring under dry nitrogen. After 1.5 h, the reaction mixture was cooled to room temperature and kept for another 16 h under dry nitrogen. The title compound was isolated as a black glassy solid in quantitative yield. Elemental analysis calculated: C, 41.7; S, 50.4; H, 3.89%. Found: C, 40.51; S, 50.11; H, 3.02% (Atlantic Microlab, Inc.).

Determination of dark sulfur content

A modified literature method for quantification of the dark sulfur content by UV-vis spectroscopy was employed to determine the dark sulfur content.[108] A 6–7 mg sample of the product of interest was weighed with a microbalance and added to 250 mL volumetric flasks with approximately 230 mL of ethyl acetate. The mixture was allowed to stir for 30 min, after which the solution was made up to the mark of 250 mL with ethyl acetate. A 3 mL aliquot of each solution was transferred into each of two cuvettes, and 3 mL pure ethyl acetate was transferred to another cuvette to serve as a blank. Absorption data were collected at 275 nm, and dark sulfur content was calculated from a calibration curve having the equation $y = 35.302x + 0.0021$ ($R^2 = 0.9992$), where y is absorbance, and x is the concentration of sulfur in mg mL^{-1}.

Conflicts of interest

There are no conflicts to declare.

Data availability

The data supporting this article have been included as part of the SI: Infrared spectra of *O*,*O*′-diallylbisphenol A, 2,4-dichloro-3,5-dimethylphenol, $DAClS_{51}$, DAS_{50}, and DS_{81}; SEM-EDS data for $DAClS_{51}$ and DAS_{50}; TGA curves for $DAClS_{51}$ and DAS_{50}; DSC traces for prepared materials; photos of specimens and different stages of reaction; DMA data and stress–strain plots for flexural strength of $DAClS_{51}$, and DAS_{50}. See DOI: https://doi.org/10.1039/d5py00548e.

Acknowledgements

This research was funded by The National Science Foundation grant number CHE-2203669.

References

1 K.-S. Kang, C. Olikagu, T. Lee, J. Bao, J. Molineux, L. N. Holmen, K. P. Martin, K.-J. Kim, K. H. Kim, J. Bang, V. K. Kumirov, R. S. Glass, R. A. Norwood, J. T. Njardarson and J. Pyun, *J. Am. Chem. Soc.*, 2022, **144**, 23044–23052.

Open Access Article. Published on 04 September 2025. Downloaded on 2/1/2026 10:21:47 PM. This article is licensed under a Creative Commons Attribution 3.0 Unported Licence.

2 C. R. Westerman and C. L. Jenkins, *Macromolecules*, 2018, **51**, 7233–7238.
3 M. S. Karunarathna, M. K. Lauer, A. G. Tennyson and R. C. Smith, *Polym. Chem.*, 2020, **11**, 1621–1628.
4 N. Gupta, P. K. Roychoudhury and J. K. Deb, *Appl. Microbiol. Biotechnol.*, 2005, **66**, 356–366.
5 US Geological Survey. (January 31, 2023). Sulfur production worldwide in 2022, by country, In *Statista*, retrieved December 27, 2023, from **https://www-statista-com.libproxy.clemson.edu/statistics/1031181/sulfur-production-globally-by-country/**.
6 A. Tanimu and K. Alhooshani, *Energy Fuels*, 2019, **33**, 2810–2838.
7 C. V. Lopez, C. P. Maladeniya and R. C. Smith, *Electrochemistry*, 2020, **1**, 226–259.
8 M. Arslan, B. Kiskan, E. C. Cengiz, R. Demir-Cakan and Y. Yagci, *Eur. Polym. J.*, 2016, **80**, 70–77.
9 P. T. Dirlam, A. G. Simmonds, T. S. Kleine, N. A. Nguyen, L. E. Anderson, A. O. Klever, A. Florian, P. J. Costanzo, P. Theato, M. E. Mackay, R. S. Glass, K. Char and J. Pyun, *RSC Adv.*, 2015, **5**, 24718–24722.
10 J. J. Griebel, G. Li, R. S. Glass, K. Char and J. Pyun, *J. Polym. Sci., Part A: Polym. Chem.*, 2015, **53**, 173–177.
11 A. Hoefling, D. T. Nguyen, Y. J. Lee, S.-W. Song and P. Theato, *Mater. Chem. Front.*, 2017, **1**, 1818–1822.
12 Z. Chen, J. Droste, G. Zhai, J. Zhu, J. Yang, M. R. Hansen and X. Zhuang, *Chem. Commun.*, 2019, **55**, 9047–9050.
13 W. J. Chung, J. J. Griebel, E. T. Kim, H. Yoon, A. G. Simmonds, H. J. Ji, P. T. Dirlam, R. S. Glass, J. J. Wie, N. A. Nguyen, B. W. Guralnick, J. Park, A. Somogyi, P. Theato, M. E. Mackay, Y.-E. Sung, K. Char and J. Pyun, *Nat. Chem.*, 2013, **5**, 518–524.
14 I. Gomez, O. Leonet, J. A. Blazquez and D. Mecerreyes, *ChemSusChem*, 2016, **9**, 3419–3425.
15 I. Gomez, D. Mecerreyes, J. A. Blazquez, O. Leonet, H. Ben Youcef, C. Li, J. L. Gomez-Camer, O. Bundarchuk and L. Rodriguez-Martinez, *J. Power Sources*, 2016, **329**, 72–78.
16 H. Kang, H. Kim and M. J. Park, *Adv. Energy Mater.*, 2018, **8**, 1802423.
17 S. Choudhury, P. Srimuk, K. Raju, A. Tolosa, S. Fleischmann, M. Zeiger, K. I. Ozoemena, L. Borchardt and V. Presser, *Sustainable Energy Fuels*, 2018, **2**, 133–146.
18 J. J. Griebel, S. Namnabat, E. T. Kim, R. Himmelhuber, D. H. Moronta, W. J. Chung, A. G. Simmonds, K.-J. Kim, J. van der Laan, N. A. Nguyen, E. L. Dereniak, M. E. MacKay, K. Char, R. S. Glass, R. A. Norwood and J. Pyun, *Adv. Mater.*, 2014, **26**, 3014–3018.
19 J. J. Griebel, N. A. Nguyen, S. Namnabat, L. E. Anderson, R. S. Glass, R. A. Norwood, M. E. MacKay, K. Char and J. Pyun, *ACS Macro Lett.*, 2015, **4**, 862–866.
20 S. Namnabat, J. J. Gabriel, J. Pyun, R. A. Norwood, E. L. Dereniak and J. van der Laan, *Proc. SPIE*, 2014, **9070**, 90702H.
21 T. S. Kleine, R. S. Glass, D. L. Lichtenberger, M. E. MacKay, K. Char, R. A. Norwood and J. Pyun, *ACS Macro Lett.*, 2020, **9**, 245–259.
22 S. Park, D. Lee, H. Cho, J. Lim and K. Char, *ACS Macro Lett.*, 2019, **8**, 1670–1675.
23 W. Cho, S. Kim and J. J. Wie, *Acc. Mater. Res.*, 2024, **5**, 625–639.
24 A. D. Tikoalu, N. A. Lundquist and J. M. Chalker, *Adv. Sustainable Syst.*, 2020, **4**, 1900111.
25 Y. Fu, C. Yang, Y. Zheng, J. Jiang, Y. Sun, F. Chen and J. Hu, *J. Mol. Liq.*, 2021, **328**, 115420.
26 H.-K. Lin, Y.-S. Lai and Y.-L. Liu, *ACS Sustainable Chem. Eng.*, 2019, **7**, 4515–4522.
27 M. W. Thielke, L. A. Bultema, D. D. Brauer, P. Theato, B. Richter and M. Fischer, *Polymers*, 2016, **8**, 1–9.
28 M. L. Eder, C. B. Call and C. L. Jenkins, *ACS Appl. Polym. Mater.*, 2022, **4**, 1110–1116.
29 T. Hasell, D. J. Parker, H. A. Jones, T. McAllister and S. M. Howdle, *Chem. Commun.*, 2016, **52**, 5383–5386.
30 M. P. Crockett, A. M. Evans, M. J. H. Worthington, I. S. Albuquerque, A. D. Slattery, C. T. Gibson, J. A. Campbell, D. A. Lewis, G. J. L. Bernardes and J. M. Chalker, *Angew. Chem., Int. Ed.*, 2016, **55**, 1714–1718.
31 M. J. H. Worthington, R. L. Kucera, I. S. Albuquerque, C. T. Gibson, A. Sibley, A. D. Slattery, J. A. Campbell, S. F. K. Alboaiji, K. A. Muller, J. Young, N. Adamson, J. R. Gascooke, D. Jampaiah, Y. M. Sabri, S. K. Bhargava, S. J. Ippolito, D. A. Lewis, J. S. Quinton, A. V. Ellis, A. Johs, G. J. L. Bernardes and J. M. Chalker, *Chem. – Eur. J.*, 2017, **23**, 16219–16230.
32 D. J. Parker, H. A. Jones, S. Petcher, L. Cervini, J. M. Griffin, R. Akhtar and T. Hasell, *J. Mater. Chem. A*, 2017, **5**, 11682–11692.
33 J.-S. M. Lee, D. J. Parker, A. I. Cooper and T. Hasell, *J. Mater. Chem. A*, 2017, **5**, 18603–18609.
34 S. Petcher, D. J. Parker and T. Hasell, *Environ. Sci.: Water Res. Technol.*, 2019, **5**, 2142–2149.
35 J. M. Scheiger, C. Direksilp, P. Falkenstein, A. Welle, M. Koenig, S. Heissler, J. Matysik, P. A. Levkin and P. Theato, *Angew. Chem., Int. Ed.*, 2020, **59**, 18639–18645.
36 J. M. Chalker, M. Mann, M. J. H. Worthington and L. J. Esdaile, *Org. Mater.*, 2021, **3**, 362–373.
37 F. G. Mueller, L. S. Lisboa and J. M. Chalker, *Adv. Sustainable Syst.*, 2023, **7**, 2300010.
38 L.-A. Ko, Y.-S. Huang and Y. A. Lin, *ACS Appl. Polym. Mater.*, 2021, **3**, 3363–3372.
39 A. S. Farioli, M. V. Martinez, C. Barbero, E. Yslas and D. Acevedo, *J. Appl. Polym. Sci.*, 2024, **141**, e54914.
40 S. Lyu, Z. Z. Abidin, T. C. S. Yaw and M. F. M. G. Resul, *Environ. Sci. Pollut. Res.*, 2024, **31**, 16940–16957.
41 N. A. Lundquist and J. M. Chalker, *Sustainable Mater. Technol.*, 2020, **26**, e00222.
42 Y. Xin, H. Peng, J. Xu and J. Zhang, *Adv. Funct. Mater.*, 2019, **29**, 1808989.
43 S. J. Tonkin, C. T. Gibson, J. A. Campbell, D. A. Lewis, A. Karton, T. Hasell and J. M. Chalker, *Chem. Sci.*, 2020, **11**, 5537–5546.
44 Y. Huang, Y. Liu, G. Si and C. Tan, *ACS Sustainable Chem. Eng.*, 2024, **12**, 2212–2224.

 This journal is © The Royal Society of Chemistry 2025

Open Access Article. Published on 04 September 2025. Downloaded on 2/1/2026 10:21:47 PM. This article is licensed under a Creative Commons Attribution 3.0 Unported Licence.

45 H. Shen, H. Qiao and H. Zhang, *Chem. Eng. J.*, 2022, **450**, 137905.
46 S. F. do Valle, A. S. Giroto, H. P. G. Reis, G. G. F. Guimarães and C. Ribeiro, *J. Agric. Food Chem.*, 2021, **69**, 2392–2402.
47 S. F. Valle, A. S. Giroto, R. Klaic, G. G. F. Guimaraes and C. Ribeiro, *Polym. Degrad. Stab.*, 2019, **162**, 102–105.
48 M. Mann, J. E. Kruger, F. Andari, J. McErlean, J. R. Gascooke, J. A. Smith, M. J. H. Worthington, C. C. C. McKinley, J. A. Campbell, D. A. Lewis, T. Hasell, M. V. Perkins and J. M. Chalker, *Org. Biomol. Chem.*, 2019, **17**, 1929–1936.
49 K. Wei, K. Zhao, Y. Gao, H. Zhang, X. Yu, M.-H. Li and J. Hu, *Chem. Eng. J.*, 2023, **462**, 142191.
50 M. K. Lauer, M. S. Karunarathna, A. G. Tennyson and R. C. Smith, *Mater. Adv.*, 2020, **1**, 590–594.
51 M. K. Lauer, M. S. Karunarathna, A. G. Tennyson and R. C. Smith, *Mater. Adv.*, 2020, **1**, 2271–2278.
52 A. D. Smith, A. G. Tennyson and R. C. Smith, *Sustain. Chem.*, 2020, **1**, 209–237.
53 C. V. Lopez, A. D. Smith and R. C. Smith, *RSC Adv.*, 2022, **12**, 1535–1542.
54 M. E. Duarte, B. Huber, P. Theato and H. Mutlu, *Polym. Chem.*, 2020, **11**, 241–248.
55 H.-K. Lin and Y.-L. Liu, *Macromol. Rapid Commun.*, 2018, **39**, 1700832.
56 Y. Liu, Y. Chen, Y. Zhang, Y. Chen, L. Wang, X. Zan and L. Zhang, *Polymers*, 2020, **12**, 2127.
57 M. J. H. Worthington, R. L. Kucera and J. M. Chalker, *Green Chem.*, 2017, **19**, 2748–2761.
58 D. Wang, Z. Tang, S. Fang, S. Wu, H. Zeng, A. Wang and B. Guo, *Carbon*, 2021, **184**, 409–417.
59 L. Sun, S. Gao, X. Gui, L. Liu, K. Xu and H. Liu, *Eur. Polym. J.*, 2020, **123**, 109440.
60 J. Lim, J. Pyun and K. Char, *Angew. Chem., Int. Ed.*, 2015, **54**, 3249–3258.
61 D. A. Boyd, *Angew. Chem., Int. Ed.*, 2016, **55**, 15486–15502.
62 S. Gwon, S.-Y. Oh and M. Shin, *Constr. Build. Mater.*, 2018, **181**, 276–286.
63 C. Wongsirathat and O. Chavalparit, *Adv. Mater. Res.*, 2014, **856**, 113–117.
64 A. E. Davis, K. B. Sayer and C. L. Jenkins, *Polym. Chem.*, 2022, **13**, 4634–4640.
65 K. B. Sayer, V. L. Miller, Z. Merrill, A. E. Davis and C. L. Jenkins, *Polym. Chem.*, 2023, **14**, 3091–3098.
66 A. M. Abraham, S. V. Kumar and S. M. Alhassan, *Chem. Eng. J.*, 2018, **332**, 1–7.
67 T. S. Kleine, N. A. Nguyen, L. E. Anderson, S. Namnabat, E. A. LaVilla, S. A. Showghi, P. T. Dirlam, C. B. Arrington, M. S. Manchester, J. Schwiegerling, R. S. Glass, K. Char, R. A. Norwood, M. E. Mackay and J. Pyun, *ACS Macro Lett.*, 2016, **5**, 1152–1156.
68 S. Akay, B. Kayan, D. Kalderis, M. Arslan, Y. Yagci and B. Kiskan, *J. Appl. Polym. Sci.*, 2017, **134**, 45306.
69 Y. Zhang, T. Kleine, K. Carothers, D. Phan, R. Glass, M. Mackay, K. Char and J. Pyun, *Polym. Chem.*, 2018, **9**, 2290–2294.
70 Y. Zhang, N. G. Pavlopoulos, T. S. Kleine, M. Karayilan, R. S. Glass, K. Char and J. Pyun, *J. Polym. Sci., Part A: Polym. Chem.*, 2019, **57**, 7–12.
71 S. Park, M. Chung, A. Lamprou, K. Seidel, S. Song, C. Schade, J. Lim and K. Char, *Chem. Sci.*, 2022, **13**, 566–572.
72 J. A. Smith, R. Mulhall, S. Goodman, G. Fleming, H. Allison, R. Raval and T. Hasell, *ACS Omega*, 2020, **5**, 5229–5234.
73 S. Zhang, P. Liu, M. Guo, Q. Yu, Y. Hu, Z. Tang, B. Guo and G. Zhou, *Compos. Sci. Technol.*, 2023, **239**, 110075.
74 Y. A. Wickramasingha, F. Stojcevski, D. J. Eyckens, D. J. Hayne, J. M. Chalker and L. C. Henderson, *Macromol. Mater. Eng.*, 2024, **309**, 2300298.
75 I. Gomez, A. F. De Anastro, O. Leonet, J. A. Blazquez, H.-J. Grande, J. Pyun and D. Mecerreyes, *Macromol. Rapid Commun.*, 2018, **39**, e1800529.
76 K. Orme, A. H. Fistrovich and C. L. Jenkins, *Macromolecules*, 2020, **53**, 9353–9361.
77 M. K. Lauer, A. G. Tennyson and R. C. Smith, *ACS Appl. Polym. Mater.*, 2020, **2**, 3761–3765.
78 C. P. Maladeniya, M. S. Karunarathna, M. K. Lauer, C. V. Lopez, T. Thiounn and R. C. Smith, *Mater. Adv.*, 2020, **1**, 1665–1674.
79 M. K. Lauer, A. G. Tennyson and R. C. Smith, *Mater. Adv.*, 2021, **2**, 2391–2397.
80 H. Berk, M. Kaya, M. Topcuoglu, N. Turkten, Y. Karatas and A. Cihaner, *React. Funct. Polym.*, 2023, **187**, 105581.
81 A. Hoefling, Y. J. Lee and P. Theato, *Macromol. Chem. Phys.*, 2017, **218**, 1600303.
82 Y. Jin, C. Hu, Z. Wang, Z. Xia, R. Li, S. Shi, S. Xu and L. Yuan, *ACS Sustainable Chem. Eng.*, 2023, **11**, 11259–11268.
83 S. Zhang, Q. Yu, P. Liu, M. Guo, J. Ren, H. Li, Y. Hu and G. Zhou, *ACS Sustainable Chem. Eng.*, 2023, **11**, 18041–18050.
84 O. Bayram, B. Kiskan, E. Demir, R. Demir-Cakan and Y. Yagci, *ACS Sustainable Chem. Eng.*, 2020, **8**, 9145–9155.
85 Q.-L. Li, X.-X. Li, H.-M. Zhang and X.-L. Sha, *Eur. Polym. J.*, 2024, **215**, 113222.
86 A. S. M. Ghumman, M. R. Shamsuddin, M. M. Nasef, W. Z. N. Yahya, M. Ayoub, B. Cheah and A. Abbasi, *ChemistrySelect*, 2021, **6**, 1180–1190.
87 Q. Ni, J. Wu, P. Kong, Y. Wang, Y. Li, Y. Li and X. Peng, *ACS Appl. Polym. Mater.*, 2022, **4**, 4689–4698.
88 J. Cubero-Cardoso, P. Gómez-Villegas, M. Santos-Martín, A. Sayago, Á. Fernández-Recamales, R. Fernández de Villarán, A. A. Cuadri, J. E. Martín-Alfonso, R. Borja, F. G. Fermoso, R. León and J. Urbano, *Polym. Test.*, 2022, **109**, 107546.
89 A. S. M. Ghumman, R. Shamsuddin, M. M. Nasef, W. Z. Nisa Yahya and A. Abbasi, *Polymer*, 2021, **219**, 123553.
90 A. Nayeem, M. F. Ali and J. H. Shariffuddin, *Mater. Today: Proc.*, 2022, **57**, 1095–1100.
91 Z. Guo, X. Jiao, K. Wei, J. Wu and J. Hu, *Green Chem.*, 2023, **25**, 4544–4552.

Open Access Article. Published on 04 September 2025. Downloaded on 2/1/2026 10:21:47 PM. This article is licensed under a Creative Commons Attribution 3.0 Unported Licence.

92 Y. Lyu and Q. Su, *Polym. Polym. Compos.*, 2023, **31**, 09673911231181255.
93 A. Gupta, M. J. H. Worthington, H. D. Patel, M. R. Johnston, M. Puri and J. M. Chalker, *ACS Sustainable Chem. Eng.*, 2022, **10**, 9022–9028.
94 C. Herrera, K. J. Ysinga and C. L. Jenkins, *ACS Appl. Mater. Interfaces*, 2019, **11**, 35312–35318.
95 X. Wu, J. A. Smith, S. Petcher, B. Zhang, D. J. Parker, J. M. Griffin and T. Hasell, *Nat. Commun.*, 2019, **10**, 10035–10044.
96 J. H. Hwang, J. M. Lee, J. H. Seo, G. Y. Noh, W. Byun, S. Kim, W. Lee, S. Park, D.-G. Kim and Y. S. Kim, *Green Chem.*, 2023, **25**, 4641–4646.
97 P. Yan, W. Zhao, F. McBride, D. Cai, J. Dale, V. Hanna and T. Hasell, *Nat. Commun.*, 2022, **13**, 4824.
98 R. Tedjini, R. Viveiros, T. Casimiro and V. D. B. Bonifácio, *RSC Mechanochem.*, 2024, **1**, 176–180.
99 L. He, J. Yang, H. Jiang, H. Zhao and H. Xia, *Ind. Eng. Chem. Res.*, 2023, **62**, 9587–9594.
100 S. Zhang, L. Pan, L. Xia, Y. Sun and X. Liu, *React. Funct. Polym.*, 2017, **121**, 8–14.
101 J. Jia, J. Liu, Z.-Q. Wang, T. Liu, P. Yan, X.-Q. Gong, C. Zhao, L. Chen, C. Miao, W. Zhao, S. Cai, X.-C. Wang, A. I. Cooper, X. Wu, T. Hasell and Z.-J. Quan, *Nat. Chem.*, 2022, **14**, 1249–1257.
102 J. Jia, P. Yan, S. D. Cai, Y. Cui, X. Xun, J. Liu, H. Wang, L. Dodd, X. Hu, D. Lester, X.-C. Wang, X. Wu, T. Hasell and Z.-J. Quan, *Eur. Polym. J.*, 2024, **207**, 112815.
103 P. Yan, W. Zhao, S. J. Tonkin, J. M. Chalker, T. L. Schiller and T. Hasell, *Chem. Mater.*, 2022, **34**, 1167–1178.
104 N. A. Lundquist, A. D. Tikoalu, M. J. H. Worthington, R. Shapter, S. J. Tonkin, F. Stojcevski, M. Mann, C. T. Gibson, J. R. Gascooke, A. Karton, L. C. Henderson, L. J. Esdaile and J. M. Chalker, *Chem. – Eur. J.*, 2020, **26**, 10035–10044.
105 V. Hanna, M. Graysmark, H. Willcock and T. Hasell, *J. Mater. Chem. A*, 2024, **12**, 1211–1217.
106 J. Bao, K. P. Martin, E. Cho, K.-S. Kang, R. S. Glass, V. Coropceanu, J.-L. Bredas, W. O. N. Parker Jr., J. T. Njardarson and J. Pyun, *J. Am. Chem. Soc.*, 2023, **145**, 12386–12397.
107 J. J. Dale, S. Petcher and T. Hasell, *ACS Appl. Polym. Mater.*, 2022, **4**, 3169–3173.
108 J. J. Dale, J. Stanley, R. A. Dop, G. Chronowska-Bojczuk, A. J. Fielding, D. R. Neill and T. Hasell, *Eur. Polym. J.*, 2023, **195**, 112198.
109 Y.-S. Lai and Y.-L. Liu, *Macromol. Rapid Commun.*, 2023, **44**, 2300014.
110 N. L. Kapuge Dona, C. P. Maladeniya and R. C. Smith, *Eur. J. Org. Chem.*, 2024, e202301269.
111 T. Thiounn, M. K. Lauer, M. S. Karunarathna, A. G. Tennyson and R. C. Smith, *Sustainable Chem.*, 2020, **1**, 183–197.
112 T. Thiounn, M. S. Karunarathna, M. K. Lauer, A. G. Tennyson and R. C. Smith, *RSC Sustainability*, 2023, **1**, 535–542.
113 M. S. Karunarathna, C. P. Maladeniya, M. K. Lauer, A. G. Tennyson and R. C. Smith, *RSC Adv.*, 2023, **13**, 3234–3240.
114 M. S. Karunarathna, A. G. Tennyson and R. C. Smith, *J. Mater. Chem. A*, 2020, **8**, 548–553.
115 M. S. Karunarathna, M. K. Lauer and R. C. Smith, *J. Mater. Chem. A*, 2020, **8**, 20318–20322.
116 K. A. Tisdale, N. L. K. Dona, C. P. Maladeniya and R. C. Smith, *J. Polym. Environ.*, 2024, **32**, 4842–4854.
117 M. S. Karunarathna and R. C. Smith, *Sustainability*, 2020, **12**, 734–748.
118 M. S. Karunarathna, M. K. Lauer, T. Thiounn, R. C. Smith and A. G. Tennyson, *J. Mater. Chem. A*, 2019, **7**, 15683–15690.
119 K. Marossy and P. Bárczy, *Polym. Polym. Compos.*, 2003, **11**, 115–122.
120 J. C. Souza, C. H. F. B. Souza, C. H. F. Silva, M. E. S. R. Silva, R. G. Sousa and R. F. S. Freitas, *Macromol. Symp.*, 2012, **319**, 150–160.

 This journal is © The Royal Society of Chemistry 2025